Synthesis and properties of a triphenylene–butadiynylene macrocycle†‡

Henning Wettach,[a] Sigurd Höger,*[a] Debangshu Chaudhuri,[b] John. M. Lupton,*[b] Feng Liu,[c] Elizabeth M. Lupton,*[c] Sergei Tretiak,[d] Guojie Wang,[e] Min Li,[e] Steven De Feyter,*[e] Steffen Fischer[f] and Stephan Förster*[f]

Received 6th July 2010, Accepted 23rd August 2010
DOI: 10.1039/c0jm02150d

The synthesis and characterization of a shape-persistent triphenylene–butadiynylene macrocycle formed by intermolecular Glaser-coupling of two "half-rings" and also by intramolecular coupling of the appropriate open dimer, respectively, are described in detail. The investigation of the photophysics has revealed that—compared to its open dimer—the macrocycle is more conjugated in the ground state and less so in the excited state, a result of the diacetylene bending in the macrocycle due to its constrained topology. The macrocycle is decorated with flexible side groups that support its adsorption on highly oriented pyrolytic graphite (HOPG) where a concentration-dependence of the 2D-structure is observed by means of scanning tunnelling microscopy (STM). The flexible side groups also guarantee a high compound solubility even in nonpolar solvents (cyclohexane). However, solvophobic interactions lead to the formation of a tube-like superstructure, as revealed by dynamic light scattering, X-ray scattering and atomic force microscopy.

Introduction

Advances in molecular electronics necessitate ever more precise control over molecular shape to yield specific physical functions. Such functionality is required both on the intramolecular level, which governs electronic properties, and with regard to physical arrangement in the ensemble. Shape-persistent macrocycles with extended π-electron conjugation are appealing systems to study this interplay between form and function: the size of the conjugated system can be scaled with respect to the overall molecular size, while maintaining shape; and, as in dendritic systems, solubility can be tuned independently of intramolecular electronic structure, ultimately allowing the construction of complex covalently bonded "supramolecular"-like structures.[1] In addition, such shape-persistent structures exhibit a high degree of isomeric purity, facilitating self-assembly to molecular superstructures in the melt and in the solid state, in solution and on surfaces.[2] Rigid macrocycles with nanometre dimensions exhibit liquid crystallinity (LC) when properly decorated with flexible alkyl chains.[3,4] In solution, they can form dimers as well as extended one-dimensional aggregates depending on the electronic nature of the substituents and, even more important, on the solvent. Some of these macrocycle aggregates are also stable in the solid state and have been analyzed by electron microscopy (EM) and atomic force microscopy (AFM).[5] In addition, the precise control over photophysical properties in combination with the generic ability of macrocycles and thus aggregates to accommodate and recognize guest molecules makes them attractive building blocks for optically active chemical sensors.[6] Guest recognition is not limited to one-dimensional superstructures. Shape-persistent macrocycles can also build up two-dimensional lattices[7] at the air–water or the air–solid and liquid–solid interface and these assemblates can bind specific guest molecules.[8]

Recently, it has also become of interest to incorporate polycyclic aromatic hydrocarbon (PAH) building blocks into the rigid macrocycle backbone because of their interesting optical properties and assembly behavior.[9] During our own studies we could show that macrocycles with dibenzonaphthacenes in their rigid backbone show a higher tendency to aggregate than their benzene-based analogs and form more stable LC phases.[4b,c] However, the dibenzonaphthacenes capable of undergoing transition metal-catalyzed coupling reactions necessary to build up the macrocycles could only be obtained in a multi-step synthesis which involves itself a Pd-catalyzed dehydrohalogenation. Therefore, a methoxy to triflate transformation was necessary that extended the overall reaction sequence.[10] In contrast, some (halogen) substituted PAHs, and here especially triphenylenes, are more facile to prepare either by oxidative coupling or by a Diels–Alder approach. Both reactions do not interfere with the presence of bromides or iodides.[11] Especially the latter reaction offers appealing building blocks for larger condensed-phase structures of well-defined electronically active units.[12]

[a]*Kekulé-Institut für Organische Chemie und Biochemie, Rheinische Friedrich-Wilhelms-Universität Bonn, Gerhard-Domagk-Str. 1, 53121 Bonn, Germany. E-mail: hoeger@uni-bonn.de*
[b]*Department of Physics and Astronomy, University of Utah, Salt Lake City, UT, 84112, USA. E-mail: lupton@physics.utah.edu*
[c]*Department of Materials Science, University of Utah, Salt Lake City, UT, 84112, USA. E-mail: lupton@eng.utah.edu*
[d]*Theoretical Division and Center for Integrated Nanotechnologies (CINT), Los Alamos National Laboratory (LANL), Los Alamos, NM, 87545, USA*
[e]*Department of Chemistry, Laboratory of Photochemistry and Spectroscopy, and Institute for Nanoscale Physics and Chemistry, Katholieke Universiteit Leuven, Celestijnenlaan 200-F, 3001 Leuven, Belgium. E-mail: Steven.DeFeyter@chem.kuleuven.be*
[f]*Universität Hamburg, Institut für Physikalische Chemie, Grindelallee 117, 20146 Hamburg, Germany. E-mail: forster@chemie.uni-hamburg.de*

† Electronic supplementary information (ESI) available: Detailed synthesis and characterization of all compounds. Additional ground state geometry calculations. See DOI: 10.1039/c0jm02150d

‡ This paper is part of a *Journal of Materials Chemistry* themed issue in celebration of the 70th birthday of Professor Fred Wudl.

Here, we explore the physical and electronic structure of a family of phenyl-substituted triphenylenes.[13] We present the synthesis and detailed photophysical, quantum chemical, and structural investigations of macrocycle **1** in solution, at the solid–liquid interface and in the bulk. We note that this compound is, effectively, the phenyl-substituted triphenylene analog to Eglinton's dibenzodehydro[12]annulene **2**, which was reported 50 years ago, offering an intriguing paradigm of scalability in shape-persistent macrocycle synthesis.[14–16]

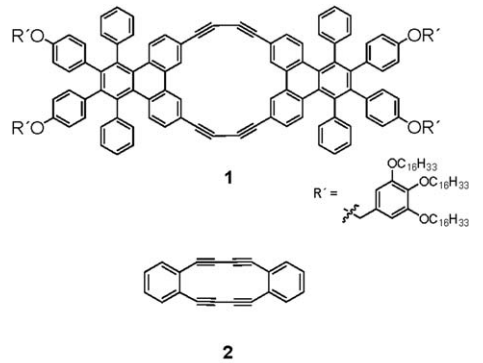

Structure of **1** and **2**

Results and discussion

Synthesis

The synthesis of the macrocycle building block is displayed in Scheme 1. 9,10-Phenanthrenequinone (**3**) was brominated yielding 3,6-dibromo-9,10-phenanthrenequinone (**4**).[17] Condensation of **4** with 1,3-diphenylacetone provides 3,6-dibromophencyclone (**5**) as diene precursor of the desired triphenylene structure.[17] Diels–Alder reaction with subsequent CO-extrusion of 3,6-dibromophencyclone (**5**) and bis-(4-methoxyphenyl)acetylene (**6**) gives 7,10-dibromo-2,3-bis-(4-methoxy-phenyl)-1,4-diphenyl-triphenylene (**7**). In order to obtain sufficient product solubility, **7** was demethylated and the resulting bis-phenol **8** alkylated with **9** to form the triphenylene **10**. Pd-catalyzed twofold Sonogashira–Hagihara coupling reaction with [(3-cyanopropyl)diisopropylsilyl]acetylene (CPDIPSA)[18] gave **11**. The CPDIPS protecting group exhibits a comparable stability to the triisopropylsilyl (TIPS) protecting group. However, the cyanopropyl substituent enhances the polarity in such a way that the separation of **11** from the educt **10** and from only partly reacted side products can be performed rather easily. In addition to that the high polarity of the CPDIPS group opens the door for the stepwise synthesis of the desired macrocycle **1**. Complete deprotection of the acetylene groups was achieved by treating **11** with tetrabutylammonium fluoride (TBAF) to give **12**.

Compound **12** was oxidatively coupled utilizing Glaser–Eglinton conditions (CuCl, $CuCl_2$, and pyridine) under pseudo high-dilution conditions (statistical approach) (Scheme 2a).[19] This was performed in such a way that a solution of the bisacetylene **12** in pyridine was slowly (96 h) added to a suspension of the copper catalyst/oxidant in the same solvent. The analysis of the crude reaction mixture was performed by analytical gel permeation chromatography (GPC) indicating that the (cyclic) dimer was the main product of the coupling reaction. It is interesting to see that here also the cyclodimer is the main product of the reaction, as it is in the case of the 1,2-diethynylbenzene coupling.[14] According to GPC analysis (Fig. 1) a small amount of the trimer was also formed along with some oligomeric and polymeric by-products. The removal of the polymeric fraction can be achieved by column chromatography on silica gel. However, a separation of cyclodimer and cyclotrimer was not possible by this procedure but required separation by preparative recycling GPC (recGPC, see ESI†).

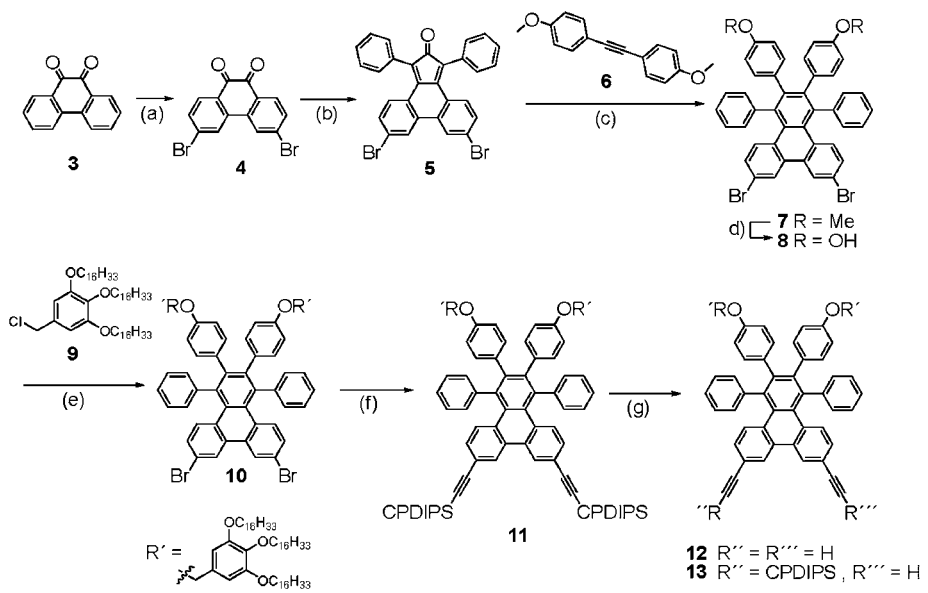

Scheme 1 (a) Br_2, nitrobenzene, 120 °C, 22 h (70%); (b) 1,3-diphenylacetone, MeOH/KOH, reflux, 30 min (80%); (c) **6**, diphenyl ether, 245 °C (55%); (d) BBr_3, −78 °C to rt (100%); (e) **9**, K_2CO_3, DMF, 65 °C, 96 h (81%); (f) [(3-cyanopropyl)diisopropylsilyl]acetylene (CPDIPSA), CuI, PPh_3, $PdCl_2(PPh_3)_2$, THF/piperidine, 65 °C, 24 h (72%); and (g) THF, 5% water, TBAF, 0 °C to rt, overnight (52% of **13**).

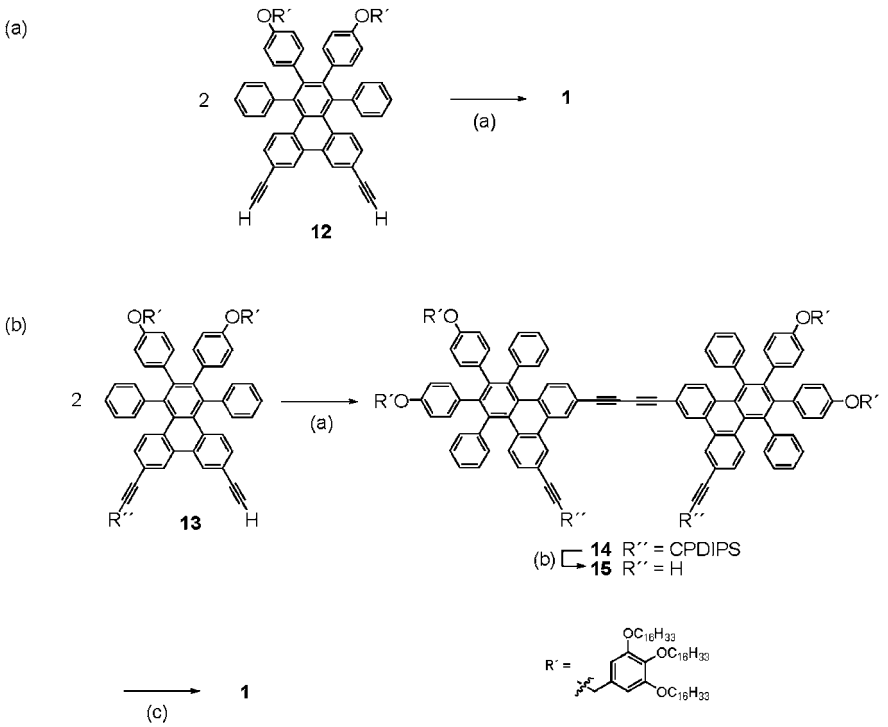

Scheme 2 (a): (a) $CuCl/CuCl_2$, pyridine, 35 °C, 120 h (53%); (b): (a) CuCl, TMEDA, O_2, CH_2Cl_2, rt, 24 h (91%); (b) TBAF, THF, rt, 1 h (95%); and (c) $CuCl/CuCl_2$, pyridine, rt, 120 h (79%).

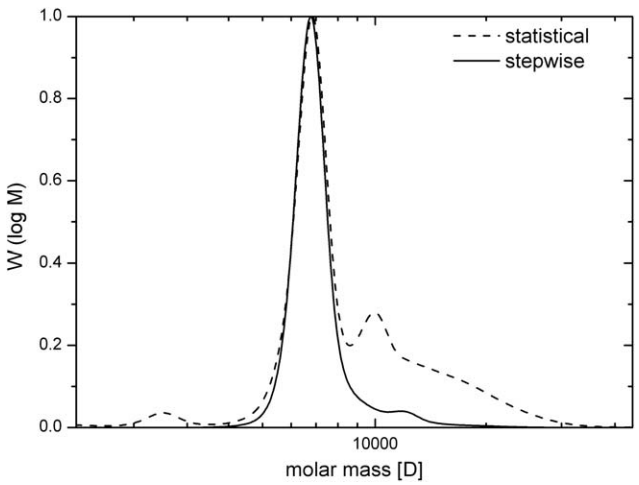

Fig. 1 Molecular weight distribution (MWD) plots of the crude products from the statistical and stepwise cyclization reactions received from GPC-measurements (*vs.* polystyrene).

Alternatively, we investigated the stepwise formation of macrocycle **1** (Scheme 2b).[14,15] When **11** is treated with equimolar amounts of TBAF in wet THF (containing 5% water) the reaction rate of the deprotection considerably slows down. Thus, it was possible to control the deprotection in such a way that the main product is the mono-deprotected compound **13**. By-products are completely deprotected bisacetylene **12** and educt **11**. Due to the great differences in polarity of the compounds containing none, one or two CPDIPS groups, the reaction progress can be easily monitored by thin layer chromatography (TLC) and product separation can be easily achieved by simple column chromatography on silica gel. Acetylene dimerization of two (mono-protected) half-ring components occurred under standard Glaser–Hay conditions (CuCl, TMEDA, and air) formed the dimeric compound **14** and subsequent deprotection of **14** yielded the bisacetylene **15**. Cu-catalyzed acetylene coupling under the same conditions as applied for the dimerization of **12** (CuCl, $CuCl_2$, pyridine, pseudo high-dilution conditions) gave macrocycle **1** in considerably higher yield than in the statistical reaction described above (Fig. 1). In this case, the MWD of the stepwise cyclization shows almost only the desired product peak and here, isolation of the product can be easily achieved by simple column chromatography on silica gel. In both cases, **1** was obtained as a faint yellow solid.[20]

Self-assembly at the liquid–solid interface

As shortly described in the introduction, the two-dimensional organization of shape-persistent macrocycles at solid interfaces is an attractive route towards complex nanostructures by the bottom-up approach. Several reports on macrocycles on the HOPG surface have been made,[7,8] and also multi-component structures that include rigid macrocycles and different guest molecules were published during the past several years.[8] In order to evaluate if **1** is also able to form ordered two-dimensional structures, we probed the self-assembly of **1** at the 1-phenyloctane–HOPG interface by scanning tunnelling microscopy (STM). Interestingly, the self-assembly behavior of the compound varies with concentration. At high concentration (2×10^{-4} M), molecules are arranged into close-packed lamella in which the π-conjugated backbones are packed side by side in a plane parallel to the graphite substrate. Only half of the alkyl

chains of the molecule are absorbed on the substrate (Type I). Yet at low concentrations (below 7×10^{-6} M), a two-dimensional porous network forms and molecules are arranged into a loose-packed lattice structure resulting in voids. Four out of six alkyl chains on each side of the molecule are absorbed (Type II). This has a pronounced effect on the molecular density: 0.100 ± 0.004 molecule per nm^2 for Type I and 0.050 ± 0.002 molecule per nm^2 for Type II. The interpretation of the concentration dependent polymorphism is discussed below.

A typical STM image of a monolayer formed upon drop-casting a 2×10^{-4} M solution of **1** in 1-phenyloctane is shown in Fig. 2. The higher tunnelling efficiency through π-electron-rich parts makes them appear higher (brighter) than the alkyl chains which are not well resolved and are located in the dark areas. A lamellar structure is formed. The distance between two adjacent molecules along the long lamella axis, a, is 1.3 ± 0.1 nm; the mean width, b, of a lamella is 7.3 ± 0.1 nm. Molecular modelling (HyperChem) shows that the π-electron-rich parts can adsorb in a plane parallel to the substrate. Those alkyl chains which can be identified adsorb parallel to one of the main symmetry directions of graphite, highlighting the important role of the substrate in templating the monolayer growth. As the distance between two alkyl chains absorbed on graphite is approximately 0.40–0.45 nm,[21] only three out of six alkyl chains on each side of the molecule are absorbed on the substrate, as illustrated in the schematic model which is superimposed on the STM image in Fig. 2. The other alkyl chains are most likely directed toward the solution phase and cannot be observed by STM. The molecular density measures 0.100 ± 0.004 molecule per nm^2 (Table 1). The unit cell contains one molecule: the plane group is $p2$. The main driving forces for the observed molecular arrangement are the van der Waals interactions between the alkyl side chains and between the alkyl chains and the substrate.[22]

Upon decreasing the concentration, a new pattern is identified. For instance, at a concentration of 7×10^{-6} M, a loose-packed lattice structure is the dominant polymorph (Fig. 3 (left)). The densely packed lamellar structure is the minority phase. Fig. 3 (right) is a typical high-resolution STM image of the open lattice structure, recorded at even lower concentration (7×10^{-8} M). The unit cell vectors a and b are 3.8 ± 0.1 and 5.8 ± 0.1 nm, respectively. The angle between a and b, α, measures $62 \pm 2°$. The increased distance between two molecules allows four alkyl chains at each side to be adsorbed in all *trans*-conformation on graphite, which is confirmed by STM imaging (Fig. 3 (right)). In this STM image, the alkyl chains are clearly identified. These

Table 1 Unit cell parameters and molecular density of monolayers of **1** determined by STM at the liquid–solid interface at various concentrations

Compound **1** in phenyloctane, concentration/$\times 10^{-6}$ M	a/nm	b/nm	α/°	Molecular density/nm^{-2}
200	1.3 ± 0.1	7.3 ± 0.1	90 ± 2	0.100 ± 0.004
7[a]	3.8 ± 0.1	5.7 ± 0.1	62 ± 2	0.050 ± 0.002
0.07	3.8 ± 0.1	5.8 ± 0.1	65 ± 2	0.050 ± 0.002

[a] Unit cell parameters refer to open lattice structure.

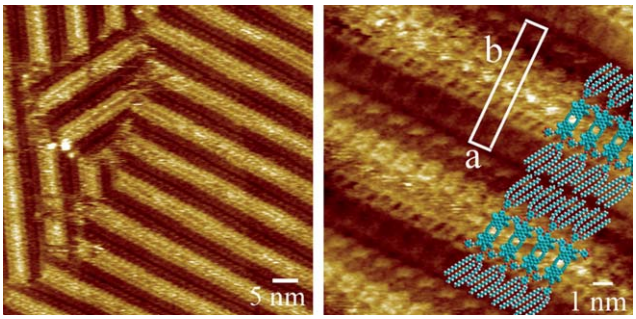

Fig. 2 Large-scale (left) and small-scale (right) STM image of a monolayer of **1** at the 1-phenyloctane–HOPG interface (2×10^{-4} M, $I_{set} = 8$ pA, and $V_{bias} = 1$ V). A unit cell and molecular models are superimposed on the STM image ($a = 1.3 \pm 0.1$ nm and $b = 7.3 \pm 0.1$ nm).

alkyl chains aligned along one of the main symmetry axes of graphite and those in adjacent rows interdigitated. The other alkyl chains, which are not visible, may possibly be adsorbed in the cavities between the molecules, or otherwise desorbed. A few molecular models illustrating the anticipated ordering of the molecules are superimposed on the STM image. The molecular density measures only 0.050 ± 0.002 molecule per nm^2 (Table 1). The unit cell contains one molecule and the plane group is $p2$. Upon decreasing the concentration, such low-density networks are observed exclusively. Typically, the voids can host solvent molecules, which are too mobile to be resolved.

The formation and structure of self-assembled monolayers at the liquid–solid interface depend on the mutual interplay between molecule–molecule interactions, molecule–solvent interactions and molecule–substrate interactions.[23] The reported concentration dependency of **1** is in line with recent studies on concentration dependent "polymorphism" for physisorbed monolayers at the liquid–solid interface. The densest polymorph is formed at the higher concentrations and self-assembly at the lower concentrations results in a porous network.[24] The adsorption–desorption equilibrium at the liquid–solid interface determines the surface coverage ratio between the dense and the open network. The concentration dependency of the self-assembling can be understood to arise from the different stability and molecular density of the two polymorphs.

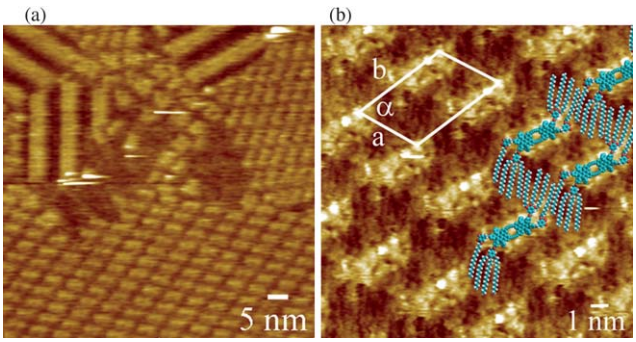

Fig. 3 STM image of a monolayer of **1** at the 1-phenyloctane–HOPG interface. Left: 7×10^{-6} M, $I_{set} = 8$ pA, and $V_{bias} = 1$ V. Right: 7×10^{-8} M, $I_{set} = 6$ pA, and $V_{bias} = 1$ V. A unit cell and molecular models are superimposed on the STM image.

Steady-state and time-resolved photoluminescence

The open dimer **15** and the macrocycle **1** offer an interesting ground to explore elementary aspects of delocalization in large π-electron systems.[16] For example, does twisting or bending have a greater impact on the energetics of the π-system? This question is crucial to understanding the microscopic nature of excited states in materials for organic electronics, such as conjugated polymers. Subtle single-molecule spectroscopic techniques have been able to identify a vast diversity of both intramolecular bending and twisting occurring within the conjugated chain.[25,26] It is not immediately obvious which of the two model compounds, the open dimer **15** or the macrocycle **1**, supports greater delocalization. In order to address these questions, we combined optical and quantum chemical investigations of the macrocycle **1** *vis-à-vis* its open dimer **15** to allow us to characterize the extent of π-electron delocalization. The difference between **1** and **15** is principally due to the increased π-delocalization in the macrocycle in the ground state. This increase is reversed in the excited state due to strong structural relaxation.

Fig. 4 shows the UV-Vis absorption and steady state photoluminescence (PL) spectra of the monomer **12** and the two dimers, **15** and **1**, in solution. For the discussion of the effect of dimerization and cyclization on the optical spectra we bear in mind that the absorption wavelength relates to the ground state electronic conformation whereas emission occurs following structural relaxation in the excited state. The lowest energy transition of **12** appears at 4.0 eV. Upon dimerization, it shifts to lower energies. However, the shift is slightly greater in the case of the macrocycle **1**, suggesting that the degree of π-delocalization is higher in **1** in the ground state. Though significantly strained, the pair of arylene bridges in **1** enforces a higher degree of coplanarity between the two triphenylene units, and thus potentially facilitates efficient delocalization throughout the molecule. In addition to the spectral shifts, important information about the excited state behavior can also be obtained from the spectral shapes. We find that the PL spectrum of **1** is a mirror image of its absorption spectrum; however, the same is not true for **15**. Such exceptions to the mirror image rule are known to result from either a structural rearrangement in the excited state or formation of lower energy excimers involving different triphenylene units.[27] In the absence of any red-shifted emission feature in the PL spectra of **15**, excimer formation can be safely ruled out.[28] A departure from the mirror image rule therefore might be a consequence of a structural rearrangement in the excited state. We speculate that owing to the molecular rigidity, **1** is far less likely to undergo any appreciable structural reorganization in the excited state, and therefore the mirror image rule holds good in its case.

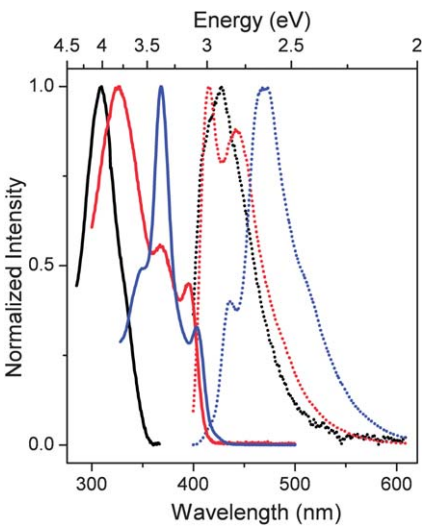

Fig. 4 Absorption (solid) and photoluminescence (dotted) spectra of the monomer **12** (black), open dimer **15** (red) and the macrocycle **1** (blue) in chloroform solution.

To test this hypothesis we applied first principles Hartree Fock calculations to determine the ground state molecular configurations, and then used configuration interaction singles (CIS) to relax the excited state geometry. Vertical transition energies were determined with the ZINDO Hamiltonian and all calculations were performed using the Gaussian program package.[29] We found that indeed the ground state of the open dimer **15** is twisted, with a dihedral angle of 41°, whereas the macrocycle **1** ensured the coplanarity of the triphenylene moieties (Fig. 5). The energy difference between the twisted and planar configurations is, however, marginal (0.0008 eV), and so the twisted conformation may not be exclusive in the ground state. For the ground state configurations we determine bright states at 3.54 eV and 3.82 eV for the open dimer which we compare to the absorption peaks at 3.37 eV and 3.79 eV respectively, and for the macrocycle we find a bright state at 3.55 eV which we associate with the peak at 3.37 eV. The lower energy transition for the open bridge is HOMO–LUMO dominated, and the transition for the macrocycle has contributions from the HOMO − 1 and LUMO + 1 as well as the HOMO and LUMO. Fig. 5 shows the computed conformations and frontier orbital plots of **1** and **15**. By examining the spatial extent of the HOMO and LUMO, we find that the orbitals reach over the ring formed by the two diacetylene bridges in **1**, thus increasing the degree of π-delocalization. Further details of the ground state geometries are given in the ESI†; it is found that the triphenylene moiety in **15** is slightly bent around a central axis, whereas a subtle asymmetric twisting occurs in **1**.

On determination of the excited state configurations (lower panel in Fig. 5) we indeed find that **15** planarizes to a dihedral angle of 8° and we find that the planar structure is 1.58 eV more stable than the twisted configuration in the excited state. Interestingly, compound **1** also relaxes with a loss of symmetry of the bridges. We determined transition energies of 2.65 eV for the open dimer and 2.55 eV for the macrocycle which we compare to the lowest energy peaks of the emission spectra at 2.80 eV and 2.64 eV, respectively. In our calculations it therefore appears that we can reproduce the configurational changes which give rise to the reversal of peak order on going from absorption to emission of **15** and **1**, respectively. Our calculations support the assumption that the significant difference between the absorption and emission spectrum of the open dimer is indeed due to a more dramatic change in the excited state configuration when compared to **1**. We note, however, that interpretation of the excited state transition energies requires a precise analysis of the relative oscillator strengths of the individual transitions, which we leave to a future detailed analysis. Suffice to say that our

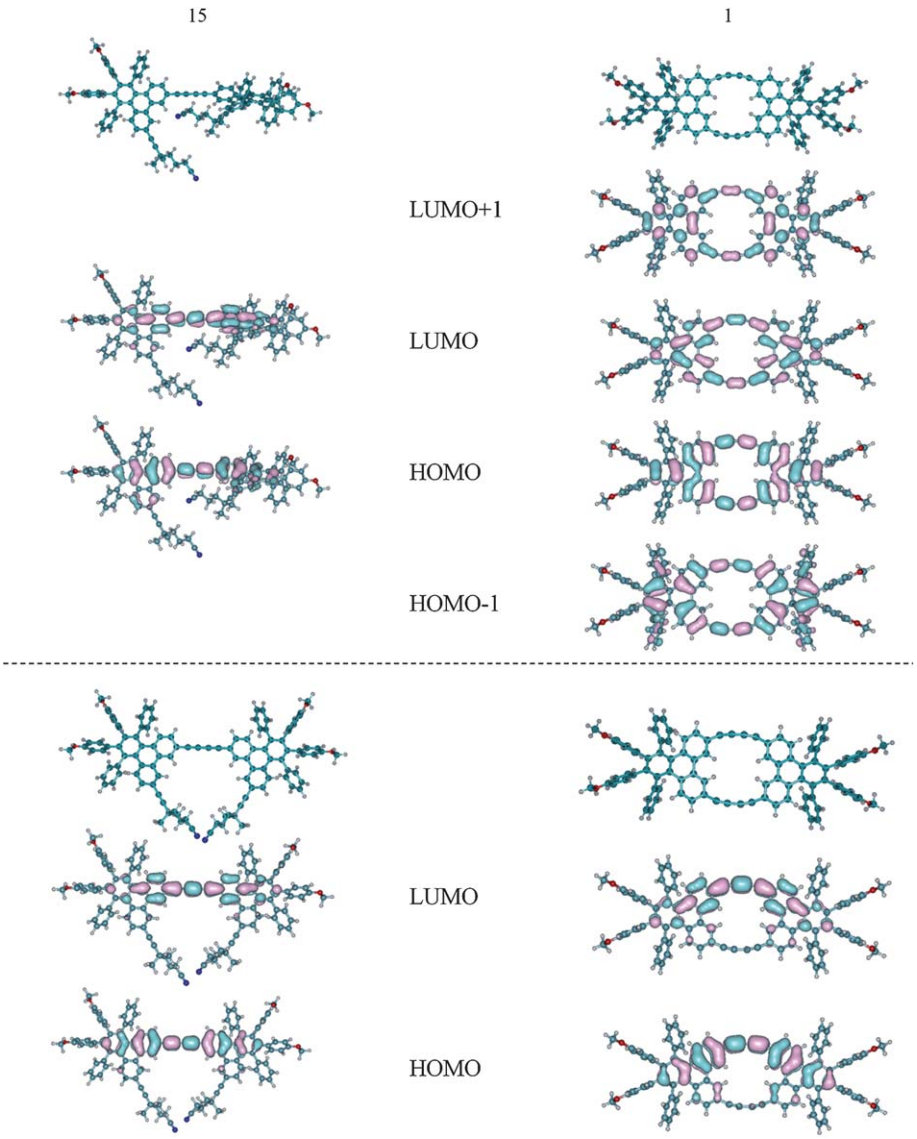

Fig. 5 Configurations and frontier orbital plots for the open dimer **15** and macrocycle **1**. The upper panel shows the ground state configuration in which **15** is twisted about the diacetylene bridge, and the frontier orbitals are delocalized over both bridges in **1**. The lower panel shows the configuration after excitation in which **15** planarizes, and the bridges in **1** are no longer symmetrical resulting in a reduction in the strength of conjugation over the longer bridge.

present results lead us to speculate that bending of the π-electron system may promote overlap between p_x and p_y orbitals, leading to an internal conversion to the lowest energy (dark) state thus promoting non-radiative decay and lowering quantum yield. This internal conversion following Kasha's rule could be reduced in the open dimer, impeding non-radiative decay (see ESI†).

A better understanding of the excited state geometry of these compounds can be developed from PL lifetime (τ) measurements. Fig. 6 presents the time resolved PL decay of the three compounds. All three exhibit a single-exponential decay. There does not appear to be any systematic correlation between τ and the degree of delocalization in the ground state. The monomer **12** shows the longest-lived PL, with a lifetime of ~8.2 ns. Among the dimers, the less delocalized **15** exhibits a faster PL decay than the more delocalized **1**. However, we observe a direct correlation between the PL decay rates and the corresponding PL quantum efficiencies (Φ). τ and Φ are related to the radiative (k_r) and non-radiative (k_{nr}) decay rate constants by $\tau^{-1} = k_r + k_{nr}$ and $\Phi = \tau \times k_r$. The values of k_r and k_{nr} calculated from the experimentally determined τ and Φ values are given in Table 2. It is interesting to note that the introduction of a second diacetylene bridge in **1** influences the radiative and non-radiative decay channels in an opposite manner. As we move from the flexible open dimer **15** to the more rigid macrocycle **1**, k_r decreases 2.7-fold. On the other hand, k_{nr} increases by a factor of 2. This trend may initially appear surprising, for one could intuitively expect the more planar macrocyclic structure to have greater oscillator strength and thus larger k_r. We note that a similar dependence of the non-radiative decay rate on the dihedral angle was recently reported for *p*-quaterphenyl derivatives which were assigned to systematic changes in electron–vibrational coupling due to shifting of ground and excited state potential surfaces.[30] It was shown that

an increased delocalization in the ground state (smaller dihedral angles) led to a faster non-radiative decay of the excited singlet state, and *vice versa*. The ratio, k_r/k_{nr}, can be related to the conjugation length (A_π*) in the excited singlet state by the expression, $A_\pi^* = \ln(k_r/k_{nr}) + 4.6$ (Å).[31] Using this expression, we calculate the excited state conjugation length for **1** and **15** as given in Table 2. Following optical excitation, the open dimer **15** undergoes significant structural reorganization in the excited state to become coplanar. The structurally rigid macrocycle **1**, on the other hand, does not undergo much structural change upon excitation. Therefore, in the excited state, where the two triphenylene units are coplanar in both **1** and **15**, a difference in the extent of delocalization is possibly governed by the strain in the diacetylene bridges (bending), rather than twisting of the π-system. From the quantum chemistry calculations we determine that in the excited state the bridges in **1** are not exactly the same length with a slight difference of 0.03 Å between them, resulting in the reduction of the strength of conjugation over the longer bridge as seen in Fig. 5. The shorter bridge in the macrocycle **1** has the same absolute length of 6.66 Å as that in **15**, but whereas in **15** the bridge is linear, in **1** the distance between triphenylene moieties is 0.30 Å less. As a consequence of this compression, the bridges in **1** are bent. We therefore conclude that strain in the bridge reduces the effective conjugation, thus increasing non-radiative decay. Increased π-conjugation in the excited state leads to a faster radiative decay, and consequently a higher quantum efficiency for **15**. To summarize, bending of the arylene bridges has a greater impact on conjugation in the excited state than in the ground state where torsion dominates; the macrocycle **1** is more conjugated in the ground state than the open dimer **15**, but less so in the excited state.

Aggregation

The aggregation of shape-persistent phenylene ethynylene macrocycles has been extensively investigated during the past decade.[5] It is generally accepted that electron accepting groups enhance the self-association while electron donating or bulky substituents disfavor the aggregation. Apart from approaches that use an alternating arrangement of electron-rich and electron-deficient aromatics, or aromatics and perfluoro aromatics, solvent effects play a highly important role in the aggregation process. The concentration dependence of the pattern formation of **1** on HOPG motivated us to investigate if an assembly of the molecules could also be observed in solution.

Fig. 7 shows the proton NMR data of **1** in dichloromethane and cyclohexane solution, respectively. In the good solvent dichloromethane, macrocycle **1** shows sharp proton signals in the aromatic and the aliphatic region as well. In cyclohexane, which is assumed to be a poor solvent for the polycyclic aromatic, the proton signals in the aromatic region flattens considerably,

Table 2 Overview of photophysical parameters of the open dimer **15** and macrocyle **1** (see text for definitions)

Sample	λ_{abs}/nm	τ/ns	Φ	k_r/ns^{-1}	k_{nr}/ns^{-1}	k_r/k_{nr}	A_π*/Å
Compound**15**	395	1.7	0.86	0.5	0.08	6.3	6.4
Compound **1**	403	2.9	0.54	0.19	0.16	1.2	4.8

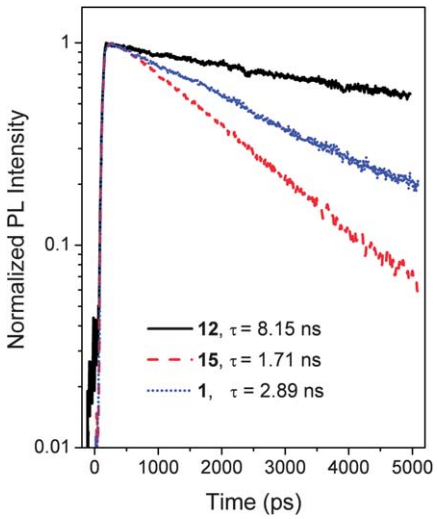

Fig. 6 Photoluminescence intensity decay of the monomer **12**, open dimer (**15**) and macrocycle (**1**).

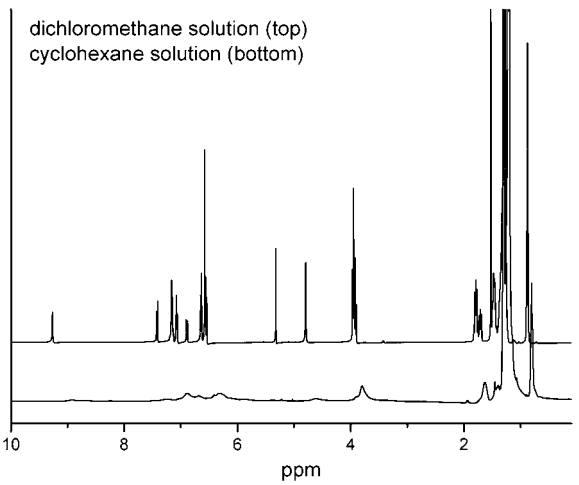

Fig. 7 Solution NMR-spectra of macrocycle **1** in dichloromethane (6.7×10^{-4} M) and cyclohexane (6.7×10^{-4} M).

representing a first indication of the self-association of **1**. However, a determination of the aggregation constant by concentration dependent NMR-chemical shift variations was not possible.

Therefore, dynamic light scattering (DLS) experiments were performed with **1** in cyclohexane and dichloromethane solutions to further investigate the aggregation behavior in different solvents (Fig. 8).[5d,32] The CONTIN analysis[33] of the autocorrelation function at a scattering angle of 90° in dichloromethane solution showed one process corresponding to a hydrodynamic radius (R_h) of approximately 1.7 nm. From the cyclohexane solution, analysis of the autocorrelation function provides a hydrodynamic radius about 3.6 nm, confirming the first indication of self-association received from the corresponding proton NMR-spectra. However, the aggregate size is not sufficiently large that extended tubular superstructures can be proposed. This result is coincident with the fact that the cyclohexane solutions do not exhibit a high viscosity, nor do they

show any birefringence. At present, we attribute this behavior to the phenyl rings in the 1- and 4-position which disfavor a strong aggregation of the macrocycles even if the compounds are twisted by 90° within a column due to the strong entropy loss.[34]

In order to obtain more information on the self-assembly of **1** in cyclohexane, we performed small-angle X-ray scattering experiments. The solutions were investigated at a concentration of 10 g L^{-1}. The measured scattering curve is shown in Fig. 9. The scattering curve can best be described by a core/shell-cylinder with a high electron density aromatic core and a low electron density alkyl shell. The solid line in Fig. 9 is a fit to the data using the form factor of a core/shell-cylinder with a homogeneous core and an inhomogeneous shell with a brush-like density profile of the form $r^{-\beta}$. The form factor $P(q)$ for such a core/shell-cylinder is given by:

$$P(q) = \langle F_{\parallel}^2(q)\rangle \langle F_{\perp}^2(q)\rangle \quad (1)$$

where $F_{\parallel}(q)$ is the longitudinal scattering amplitude parallel to the cylinder axis. $F_{\perp}(q)$ is the contribution from the cross-section of the cylinder given by:

$$F_{\perp}(q) = \frac{\left[\frac{1}{2}F(0,R_c,q) - \frac{\rho}{(2-\beta)}F(\beta,R_c,q) + \frac{\rho p^{\beta-2}}{(2-\beta)}F(\beta,R_m,q)\right]}{\left[\frac{1}{2} - \frac{\rho}{(2-\beta)} + \frac{\rho p^{\beta-2}}{(2-\beta)}\right]}$$

with $F(\beta,R,q) = {}^1F_2\left[\frac{2-\beta}{2},\ 1,\ \frac{4-\beta}{2};\ -\frac{q^2R^2}{4}\right]$ being the hypergeometric function where ρ is the core/shell electron density ratio and $p = R_c/R_m$ the ratio of core-radius to outer radius of the cylinder. The longitudinal scattering amplitude is given by $F_{\parallel}(q) = \frac{2}{qL}\mathrm{Si}[qL] - \left(\frac{\sin(qL/2)}{qL/2}\right)^2$ with Si[z] being the sine-integral. The averages $\langle\ldots\rangle$ are calculated over a Schulz–Zimm-type distribution of radii. The details of the calculations have been described previously.[35]

The form factor $P(q)$ (eqn (1)) was fitted to the measured scattering curve using a Simplex-algorithm. As a result we obtain

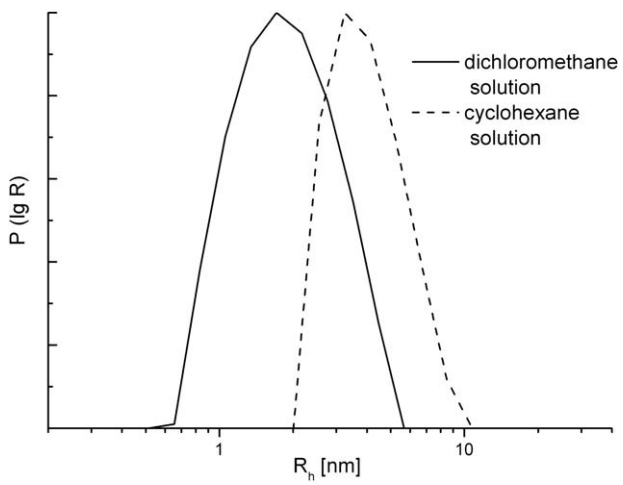

Fig. 8 CONTIN-fit of DLS-derived relaxation time distribution of **1** in dichloromethane (3.1×10^{-4} M) and cyclohexane (3.1×10^{-4} M).

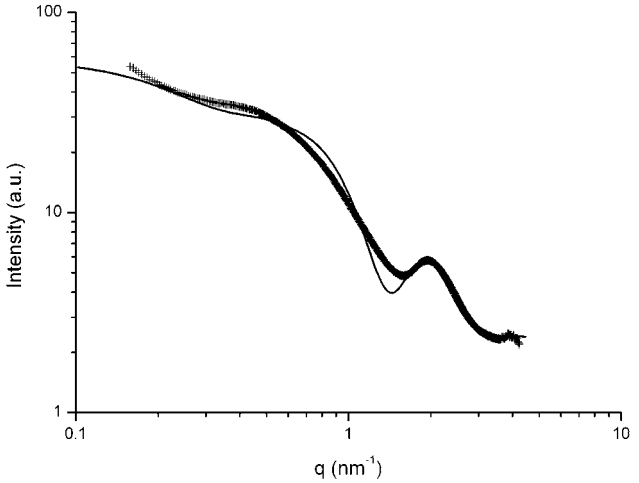

Fig. 9 Small-angle X-ray scattering curve of **1** measured in cyclohexane at a concentration of 2.2×10^{-3} M. The solid line is a fit to the data using a model of a core/shell-cylinder consisting of a high electron density aromatic core and a low electron density alkyl shell.

a cylinder core radius $R_c = 2.7$ nm, an outer radius of $R_m = 3.9$ nm, an electron density ratio of $\rho = -0.56$ and an exponent for the radial density profile of $\beta = 0.93$. The negative value of the density ratio indicates that the aromatic core has a higher and the alkyl shell a lower electron density compared to the solvent cyclohexane. The value of β is close to the value of $\beta = 1$ expected for stiff elongated alkyl chains extending from a cylindrical core. The core/shell-structure is schematically shown in Fig. 10. Many other models such as spheres and disks with core/shell-structure were also investigated, but the core/shell-cylindrical model gave by far the best agreement with the experimental data.

The small-angle X-ray scattering data therefore suggest that in cyclohexane **1** self-assembles by stacking into short cylinders (as suggested by the DLS measurements). The value of the core radius and outer radius is in good agreement with the dimensions of a cylindrical aggregate with the aromatic groups forming the core and the alkyl chains forming the shell. It is also in good agreement with the structures observed in the STM measurements and the AFM investigations (see below).

If **1** assembles into cylindrical structures in dilute solution, it could be expected that the cylinders assemble into a hexagonal arrangement upon evaporation of the solvent. For such a bulk sample we obtained the SAXS-curve as shown in Fig. 11. We observe three rather broad maxima at $q = 1.25$ nm^{-1}, $q = 2.4$ nm^{-1}, and $q = 3.3$ nm^{-1} together with a weak reflection at $q = 3.7$ nm^{-1}. This is an unusual set of reflections, indicating lower dimensional, *i.e.* one- or two-dimensional packing of objects. A scattering curve that captures the main features of the experimental curve is shown by the solid line in Fig. 11. It is calculated for the model given in Fig. 10b, where homogeneous cylinders are packed in a hexagonal array. The positions of the corresponding reflections are indicated. The solid line is calculated as:

$$I(q) = I_0 P(q) S(q) \quad (2)$$

$$S(q) = 1 + \beta(q)(Z_0(q) - 1)G(q)$$

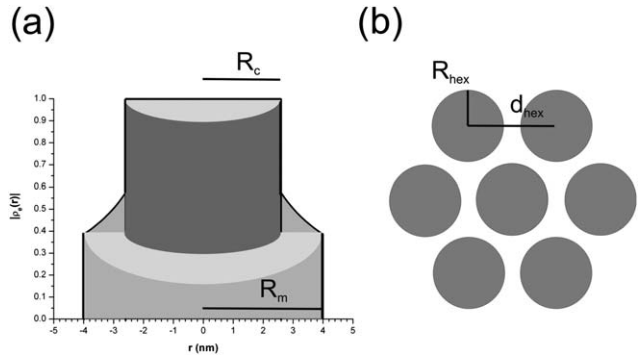

Fig. 10 (a) Density profile of the core/shell-cylinders observed in dilute solution in cyclohexane. The core radius is $R_c = 2.7$ nm and the outer radius is $R_m = 3.9$ nm. The density profile in the shell decays as $r^{-0.92}$ (b) hexagonal arrangement of cylinders observed in the dry state. The cylinder radius $R_{hex} = 2.4$ nm and the distance between two cylinders is $d_{hex} = 5.8$ nm.

where I_0 is a proportionality factor related to primary beam intensity, scattering contrast and number density, $P(q)$ is the form factor of a cylinder, $S(q)$ is the structure factor given by a set of reflections related to the lattice factor $Z_0(q)$, the Debye–Waller factor $G(q)$, and a fluctuation term $\beta(q)$. Details of the calculation are given elsewhere.[36]

We observe the first five reflections (10), (11), (20), (21), and (30) of a hexagonal lattice, where the (11) and (20) reflections appear to be merged into one broad peak. The cylinder radius is $R_{hex} = 2.4$ nm and the distance between two cylinders is $d_{hex} = 5.8$ nm with the expected size reduction, *i.e.* $R_{hex} < R_c$ and $d_{hex} < 2R_m$ when going from the solvent swollen state to the dry state. This suggests that the cylindrical aggregates are sufficiently stable to assemble into a regular hexagonal lattice in the bulk state.

The self-assembly of **1** into tubular aggregates was additionally investigated by means of atomic force microscopy (AFM). As shown before, STM at a liquid–solid interface only reveals monolayer structures or in some exceptional cases, multilayer formation. However, to detect and identify self-assembled objects formed upon drop-casting and solvent evaporation, AFM is a better tool. It turns out that **1** forms fiber-like features on HOPG when deposited from chloroform and cyclohexane following solvent evaporation, as shown in Fig. 12. The initial concentration of both solutions was 3.3×10^{-5} M. The "fibers" are longer when deposited from chloroform than from cyclohexane, which could be due to the influence of the solvent.[37] For instance, the surface tensile force (or contact angle), the solvent evaporation rate, and the specific molecule–solvent interactions can affect the assembling process.

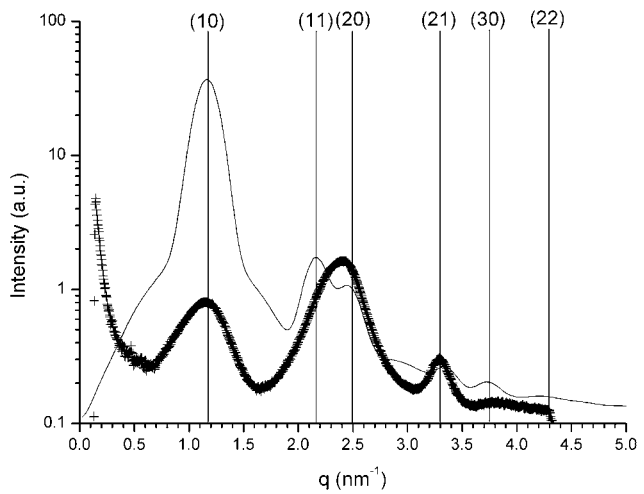

Fig. 11 Scattering curve of the sample in the dry state. The scattering curve can be described by a hexagonal array of cylinders with relatively small ordered domain sizes leading to the observed considerable peak broadening, as illustrated by the calculated curve (solid line).

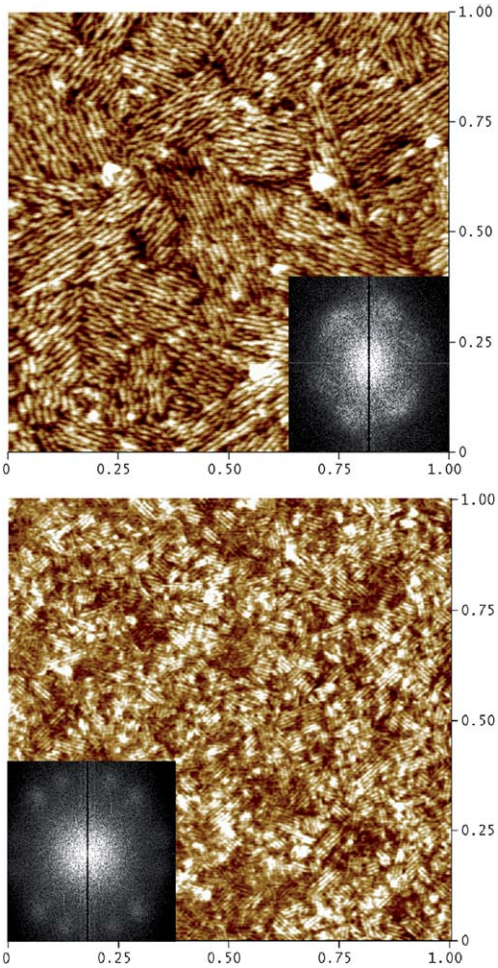

Fig. 12 Tapping-mode topography AFM image and 2D-FFT graph (inset) of **1** deposited from chloroform on HOPG. The center-to-center distance between adjacent fibers is about 13.8 nm (top). Tapping-mode topography AFM image and 2D-FFT graph (inset) of **1** deposited from cyclohexane on HOPG. The center-to-center distance between adjacent rows is about 8.7 nm (bottom).

The spots in the two-dimensional-fast Fourier transform (2D-FFT) graphs of AFM images recorded on samples prepared from chloroform show a roughly hexagonal order (Fig. 12). However, the spots are broad which suggests a distribution of orientations around 60°. The spots in the 2D-FFT graphs from AFM images recorded on samples prepared from cyclohexane

are more distinct, and 12 spots can be recognized in the 2D-FFT graphs of the lower panel in Fig. 12. Basically, these 2D-FFT graphs show two sets of hexagonal patterns, rotated with respect to each other by about 22 ± 1°.

In both cases, the 2D-FFT graphs clearly indicate the importance of substrate–molecule interactions in affecting the growth direction of the fibers. This also suggests that the fibers are not merely deposited from solution but that they are formed at the liquid–solid interface. The two subsets in the 2D-FFT graphs for AFM images of samples deposited from cyclohexane are a clear signature that the fibers are not aligned along one of the symmetry directions of graphite. Most likely, the fiber's long axis runs at an angle of 11 ± 1° with respect to a symmetry direction of graphite.

The center-to-center distance between adjacent fibers is quite different: about 13.8 nm from a chloroform solution and 8.7 nm from a cyclohexane solution, respectively. The molecular dimensions of **1** are displayed in Fig. 13. The calculated size corresponds well with the results from the STM investigations and with the observed fiber size in solution.[38]

In cyclohexane, we suggest that the fibers are formed from parallel organization of the tubular 1D stacks. Surprisingly, also a coincidence with the results from the light scattering and from the X-ray scattering in terms of the restricted cylinder length is found. On the other hand, the structures formed from chloroform are much harder to interpret and at present it is not clear if dimers of the tubular aggregates or even trimers of those aggregates are observed under the conditions we applied for the AFM measurements. Dimers and trimers of aggregates have previously been also observed on similar systems.[39]

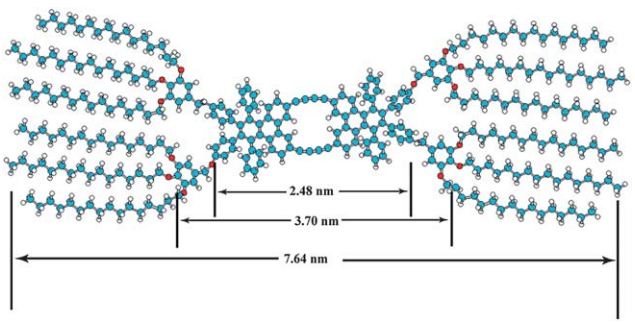

Fig. 13 Calculated molecular dimensions of **1** (HyperChem).

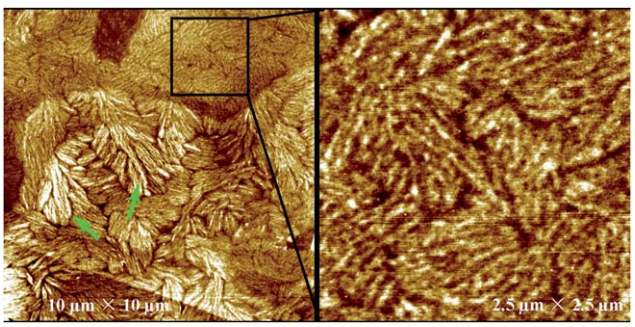

Fig. 14 Tapping-mode topography AFM image of **1** deposited from 1-phenyloctane on HOPG. The width of the fiber in the right image is 31.6 ± 3.3 nm.

Nevertheless, to approach the conditions used for the scanning tunneling microscopy experiments, upon drop casting a 1×10^{-4} M solution of **1** in phenyloctane on the basal plane of graphite, and after evaporation of the solvent over 22 hours, the film formation was investigated. In certain areas fiber-like features were observed, which often appeared to be part of dense networks as shown in the right image of Fig. 14. The width of a fiber is 31.6 ± 3.3 nm which is much larger than that formed in chloroform and cyclohexane, indicating a more complicated stacking mode. In addition, **1** tends to grow structures developing into the third dimension (3D) in some domains as pointed out by the green arrows in the left image of Fig. 14. Samples prepared at a lower concentration show patches or islands forming (not shown). The height of such films was measured to be 1.0 ± 0.2 nm, which indicates that in those regions **1** is oriented with its macrocycle unit perpendicular to the substrate.

Clearly, the self-assembly of these macrocycles is not only concentration dependent, but shows in addition to a solvent dependency, also interface dependent phenomena. The fact that the STM and AFM experiments reveal different kinds of nanostructures might be surprising initially despite the fact that samples were prepared in a similar way (concentration, substrate, and solvent). Note though that the AFM samples were investigated at the air/solid interface upon evaporation of the solvent, while the STM experiments were carried out at the liquid/solid interface. So, there is an important concentration effect on the final nanostructures. In addition, one should take into account the difference in the way STM and AFM are probing the surfaces. In STM, objects larger than a few Angstrom in height will be pushed away by the tip while such objects can be easily revealed by AFM.

Conclusion

In summary, we have synthesized a shape-persistent triphenylene–butadiynylene macrocycle by two different routes using the well-known Glaser-coupling as cyclization reaction. The macrocycle adsorbs on HOPG to form well-ordered 2D-structures, however, the density of the packing depends on the concentration of the supernatant phenyloctane solution. The photophysical investigation of the macrocycle and its open precursor has revealed that the macrocycle is more conjugated in the ground state and less so in the excited state, a result of the diacetylene bending in the macrocycle due to its constrained topology. The flexible side groups also guarantee a high compound solubility even in nonpolar solvents (cyclohexane). However, solvophobic interactions lead to the formation of tube-like superstructures that were identified by scattering methods as well as by AFM.

Acknowledgements

Financial support by the Deutsche Forschungsgemeinschaft (DFG), the SFB 624, the MIWFT in the frame of the consortium ENQUETE, the Volkswagen Foundation (JML and SH), K.U. Leuven (GOA), Fund for Scientific Research—Flanders (F.W.O.) and the Belgian Federal Science Policy Office through IAP-6/27 is gratefully acknowledged. EML and JML

acknowledge support through a LANL-CINT user project. JML is a David and Lucile Packard Foundation Fellow.

Notes and references

1 As it holds also for linear rigid structures, shape-persistent cyclic structures have to be decorated with side groups that guarantee processability, either from solution or from the melt: (*a*) W. Kern, M. Seibel and H. O. Wirth, *Makromol. Chem.*, 1959, **29**, 164; (*b*) H. A. Staab, H. Bräunling and K. Schneider, *Chem. Ber.*, 1968, **101**, 879.

2 (*a*) J. S. Moore, *Acc. Chem. Res.*, 1997, **30**, 402; (*b*) S. Höger, *J. Polym. Sci., Part A: Polym. Chem.*, 1999, **37**, 2685; (*c*) M. M. Haley, J. J. Pak and S. C. Brand, *Top. Curr. Chem.*, 1999, **201**, 81; (*d*) C. Grave and A. D. Schlüter, *Eur. J. Org. Chem.*, 2002, 3075; (*e*) Y. Yamaguchi and Z. Yoshida, *Chem.–Eur. J.*, 2003, **9**, 5430; (*f*) J. A. Marsden, G. J. Palmer and M. M. Haley, *Eur. J. Org. Chem.*, 2003, 2355; (*g*) D. Zhao and J. S. Moore, *Chem. Commun.*, 2003, 807; (*h*) S. Höger, *Chem.–Eur. J.*, 2004, **10**, 1320; (*i*) W. Zhang and J. S. Moore, *Angew. Chem.*, 2006, **118**, 4524.

3 (*a*) J. Zhang and J. S. Moore, *J. Am. Chem. Soc.*, 1994, **116**, 2655; (*b*) O. Mindyuk, M. R. Stetzer, P. A. Heiney, J. C. Nelson and J. S. Moore, *Adv. Mater.*, 1998, **10**, 1363; (*c*) M. Fischer, G. Lieser, A. Rapp, I. Schnell, W. Mamdouh, S. De Feyter, F. C. De Schryver and S. Höger, *J. Am. Chem. Soc.*, 2004, **126**, 214; (*d*) S. H. Seo, H. Seyler, J. O. Peters, T. V. Jones, T. H. Kim, J. Y. Chang and G. N. Tew, *J. Am. Chem. Soc.*, 2006, **128**, 9264; (*e*) W. Pisula, M. Kastler, C. Yang, V. Enkelmann and K. Müllen, *Chem.–Asian J.*, 2007, **2**, 51; (*f*) H. Shimura, M. Yoshio and T. Kato, *Org. Biomol. Chem.*, 2009, **7**, 3205.

4 (*a*) S. Höger, V. Enkelmann, K. Bonrad and C. Tschierske, *Angew. Chem.*, 2000, **112**, 3256; (*b*) S. Höger, X. H. Cheng, A.-D. Ramminger, V. Enkelmann, A. Rapp, M. Mondeshki and I. Schnell, *Angew. Chem.*, 2005, **117**, 2862; (*c*) S. Höger, J. Weber, A. Leppert and V. Enkelmann, *Beilstein J. Org. Chem.*, 2008, **4**, 1.

5 (*a*) J. Zhang and J. S. Moore, *J. Am. Chem. Soc.*, 1992, **114**, 9701; (*b*) A. S. Shetty, J. Zhang and J. S. Moore, *J. Am. Chem. Soc.*, 1996, **118**, 1019; (*c*) Y. Tobe, A. Nagano, K. Kawabata, M. Sonoda and K. Naemura, *Org. Lett.*, 2000, **2**, 3265; (*d*) S. Rosselli, A.-D. Ramminger, T. Wagner, B. Silier, S. Wiegand, W. Häußler, G. Lieser, V. Scheumann and S. Höger, *Angew. Chem.*, 2001, **113**, 3234; (*e*) K. Nakamura, H. Okubo and M. Yamaguchi, *Org. Lett.*, 2001, **3**, 1097; (*f*) Y. Tobe, N. Utsumi, K. Kawabata, A. Nagano, K. Adachi, S. Araki, M. Sonoda, K. Hirose and K. Nakamura, *J. Am. Chem. Soc.*, 2002, **124**, 5350; (*g*) D. Zhao and J. S. Moore, *J. Org. Chem.*, 2002, **67**, 3548; (*h*) S. Rosselli, A.-D. Ramminger, T. Wagner, G. Lieser and S. Höger, *Chem.–Eur. J.*, 2003, **9**, 3481; (*i*) Y. Saiki, H. Sugiura, K. Nakamura, M. Yamaguchi, T. Hoshi and J. Anzai, *J. Am. Chem. Soc.*, 2003, **125**, 9268; (*j*) C. T. L. Ma and M. J. MacLachlan, *Angew. Chem.*, 2005, **117**, 4250; (*k*) L. Shu and M. Mayor, *Chem. Commun.*, 2006, 4134; (*l*) H. Enozawa, M. Hasegawa, D. Takamatsu, K. Fukui and M. Iyoda, *Org. Lett.*, 2006, **8**, 1917; (*m*) C. Couet and M. Biesalski, *Soft Matter*, 2006, **2**, 1005; (*n*) P. Flores, P. Guadarrama, E. Ramos and S. Fomine, *J. Phys. Chem. A*, 2008, **112**, 3996; (*o*) J.-K. Kim, E. Lee, M.-C. Kim, E. Sim and M. Lee, *J. Am. Chem. Soc.*, 2009, **131**, 17768.

6 T. Naddo, Y. Che, W. Zhang, K. Balakrishnan, X. Yang, M. Yen, J. Zhao, J. S. Moore and J. Zang, *J. Am. Chem. Soc.*, 2007, **129**, 6978.

7 (*a*) J. Kromer, I. Rios-Carreras, G. Fuhrmann, C. Musch, M. Wunderlin, T. Debaerdemacker, E. Mena-Osteritz and P. Bäuerle, *Angew. Chem.*, 2000, **112**, 3623; (*b*) S. Höger, K. Bonrad, A. Mourran, U. Beginn and M. Möller, *J. Am. Chem. Soc.*, 2001, **123**, 5651; (*c*) D. Borissov, A. Ziegler, S. Höger and W. Freyland, *Langmuir*, 2004, **20**, 2781; (*d*) C. Grave, D. Lentz, A. Schäfer, P. Samori, J. P. Rabe, P. Franke and A. D. Schlüter, *J. Am. Chem. Soc.*, 2003, **125**, 6907; (*e*) M. Fischer, G. Lieser, A. Rapp, I. Schnell, W. Mamdouh, S. De Feyter, F. C. De Schryver and S. Höger, *J. Am. Chem. Soc.*, 2004, **126**, 214; (*f*) V. Kalsani, H. Ammon, F. Jäckel, J. P. Rabe and M. Schmittel, *Chem.–Eur. J.*, 2004, **10**, 5841; (*g*) A. Ziegler, W. Mamdouh, A. V. Heyen, M. Surin, H. Uji-i, M. M. S. Abdel-Mottaleb, F. C. De Schryver, S. De Feyter, R. Lazzaroni and S. Höger, *Chem. Mater.*, 2005, **17**, 5670; (*h*) S. Furukawa, H. Uji-i, K. Tahara, T. Ichikawa, M. Sonoda, F. C. De Schryver, Y. Tobe and S. De Feyter, *J. Am. Chem. Soc.*, 2006, **128**, 3502; (*i*) S.-H. Jung, W. Pisula, A. Rouhanipour, H. J. Räder, J. Jacob and K. Müllen, *Angew. Chem.*, 2006, **118**, 4801; (*j*) K. Tahara, C. A. Johnson, II, T. Fujita, M. Sonoda, F. C. De Schryver, S. De Feyter, M. M. Haley and Y. Tobe, *Langmuir*, 2007, **23**, 10190; (*k*) M. Schmittel, V. Kalsani, C. Michel, P. Mal, H. Ammon, F. Jäckel and J. P. Rabe, *Chem.–Eur. J.*, 2007, **13**, 6223; (*l*) S. Lei, K. Tahara, F. C. De Schryver, M. Van der Auweraer, Y. Tobe and S. De Feyter, *Angew. Chem.*, 2008, **120**, 3006; (*m*) S.-S. Jester, N. Shabelina, S. M. Le Blanc and S. Höger, *Angew. Chem.*, 2010, **122**, 6237.

8 (*a*) G.-B. Pan, X.-H. Cheng, S. Höger and W. Freyland, *J. Am. Chem. Soc.*, 2006, **128**, 4218; (*b*) E. Mena-Osteritz and P. Bäuerle, *Adv. Mater.*, 2006, **18**, 447; (*c*) S. Furukawa, K. Tahara, F. C. De Schryver, M. van der Auweraer, Y. Tobe and S. De Feyter, *Angew. Chem.*, 2007, **119**, 2889; (*d*) K. Tahara, S. Lei, D. Mössinger, H. Kozuma, K. Inukai, M. Van der Auwaerar, F. C. De Schryver, S. Höger, Y. Tobe and S. De Feyter, *Chem. Commun.*, 2008, 3897; (*e*) K. Tahara, S. Lei, W. Mamdouh, Y. Yamaguchi, T. Ichikawa, H. Uji-i, M. Sonoda, K. Kirose, F. C. De Schryver, S. De Feyter and Y. Tobe, *J. Am. Chem. Soc.*, 2008, **130**, 6666; (*f*) S. Lei, K. Tahara, X. Feng, S. Furukawa, F. C. De Schryver, K. Müllen, Y. Tobe and S. De Feyter, *J. Am. Chem. Soc.*, 2008, **130**, 7119; (*g*) B. Schmaltz, A. Rouhanipour, H. J. Räder, W. Pisula and K. Müllen, *Angew. Chem.*, 2009, **121**, 734; (*h*) T. Chen, G.-B. Pan, H. Wettach, M. Frtitzsche, S. Höger, L.-J. Wan, H.-B. Yang, B. H. Nortrop and P. J. Stang, *J. Am. Chem. Soc.*, 2010, **132**, 1328.

9 (*a*) W. J. Liu, Y. Zhou, Q.-F. Zhou, Y. Ma and J. Pei, *Org. Lett.*, 2008, **10**, 2123; (*b*) J. M. W. Chan, J. R. Tischler, S. E. Kooi, V. Bulović and T. M. Swager, *J. Am. Chem. Soc.*, 2009, **131**, 5659; (*c*) D. Wang, J. F. Hsu, M. Bagui, V. Dusevich, Y. Wang, Y. Liu, A. J. Holder and Z. Peng, *Tetrahedron Lett.*, 2009, **50**, 2147; (*d*) C. Chou, D. Wang, J. F. Hsu, Y. Liu and Z. Peng, *Synth. Met.*, 2009, **159**, 1657.

10 Functionalized phenyl dibenzo[*fg*,*op*]napthacenes were prepared from the corresponding 1,3-di(2-bromophenyl)-2,5-diarylbenzenes *via* Pd(0)-catalyzed dehydrohalogenation: (*a*) X. H. Cheng, S. Höger and D. Fenske, *Org. Lett.*, 2003, **5**, 2587; (*b*) X. Cheng, A. Ver Heyen, W. Mamdouh, H. Uji-I, F. De Schryver, S. Höger and S. De Feyter, *Langmuir*, 2007, **23**, 1281, The tetraphenylbenzenes were obtained from the condensation of pyrylium salts with phenyl acetates as described by Zimmermann and Fischer: T. Zimmermann and G. W. Fischer, *J. Prakt. Chem.*, 1987, **329**, 975.

11 (*a*) W. Dilthey, S. Henkels and A. Schäfer, *Ber. Dtsch. Chem. Ges. B*, 1938, **71**, 974; (*b*) R. A. Pascal, Jr, D. Van Engen, B. Kahr and W. D. McMillan, *J. Org. Chem.*, 1988, **53**, 1687; (*c*) W. Ried and V. B. Saxena, *Justus Liebigs Ann. Chem.*, 1970, **739**, 159.

12 (*a*) H. M. Duong, M. Bendikov, D. Steiger, Q. Zhang, G. Sonmez, J. Yamada and F. Wudl, *Org. Lett.*, 2003, **5**, 4433; (*b*) R. A. Pascal, *Chem. Rev.*, 2006, **106**, 4809; (*c*) M. Saleh, M. Baumgarten, A. Mavrinskiy, T. Schäfer and K. Müllen, *Macromolecules*, 2010, **43**, 137.

13 For triphenylene based electrooptical active compounds see, *e.g.*: (*a*) S.-i. Kawano, C. Yang, M. Ribas, S. Baluschev, M. Baumgarten and K. Müllen, *Macromolecules*, 2008, **41**, 7933; (*b*) M. Saleh, Y.-S. Park, M. Baumgarten, J.-J. Kim and K. Müllen, *Macromol. Rapid Commun.*, 2009, **30**, 1279; (*c*) T. Qin, G. Zhou, H. Scheiber, R. E. Bauer, M. Baumgarten, C. E. Anson, E. J. W. List and K. Müllen, *Angew. Chem.*, 2008, **120**, 8416; (*d*) H. Wettach, S. S. Jester, A. Colsmann, U. Lemmer, N. Rehmann, K. Meerholz and S. Höger, *Synth. Met.*, 2010, **160**, 691.

14 (*a*) G. Eglinton and A. R. Galbraith, *Proc. Chem. Soc., London*, 1957, 350; (*b*) O. M. Behr, G. Eglinton and R. A. Raphael, *Chem. Ind.*, 1959, 699; (*c*) O. M. Behr, G. Eglinton, A. R. Galbraith and R. A. Raphael, *J. Chem. Soc.*, 1960, 3614; (*d*) Q. Zhou, P. J. Carroll and T. M. Swager, *J. Org. Chem.*, 1994, **59**, 1249.

15 (*a*) S. Ott and R. Faust, *Chem. Commun.*, 2004, 388; (*b*) T. Nishinaga, N. Nodera, Y. Miyata and K. Komatsu, *J. Org. Chem.*, 2002, **67**, 6091; (*c*) U. H. F. Bunz and V. Enkelmann, *Chem.–Eur. J.*, 1999, **5**, 263.

16 For phthalocyaninodehydroannulenes and subphthalocyaninodehydroannulenes see, *e.g.*: (*a*) M. J. Cook and M. J. Heeney, *Chem.–Eur. J.*, 2006, **6**, 3958; (*b*) E. M. García-Frutos, F. Fernández-Lázaro, E. M. Maya, P. Vázquez and T. Torres, *J. Org. Chem.*, 2000, **65**, 6841; (*c*) R. S. Iglesias, C. G. Claessens, M. Á. Harranz and T. Torres, *Org. Lett.*, 2007, **9**, 5381.

17 R. Callahan, K. Marshall, R. Rothchild and K. Rosmarion, *Chem. Educ.*, 2001, **6**, 227.
18 G. Gaefke and S. Höger, *Synthesis*, 2008, **14**, 2155.
19 (*a*) C. Glaser, *Ber. Dtsch. Chem. Ges.*, 1869, **2**, 422; (*b*) F. Sondheimer and R. Wolovsky, *J. Am. Chem. Soc.*, 1962, **84**, 260; (*c*) F. Sondheimer, *Acc. Chem. Res.*, 1972, **3**, 81; (*d*) D. O'Krongly, S. R. Denmeade, M. Y. Chiang and R. Breslow, *J. Am. Chem. Soc.*, 1985, **107**, 5544; (*e*) K. Kadei and F. Vögtle, *Chem. Ber.*, 1991, **124**, 909; (*f*) S. Höger and V. Enkelmann, *Angew. Chem.*, 1995, **107**, 2917; (*g*) P. Siemsen, R. C. Livingston and F. Diederich, *Angew. Chem.*, 2000, **112**, 2740.
20 It is interesting to note that the ^{1}H-NMR signal of the intraannular proton of **1** is remarkably downfield shifted (by about 0.7 ppm) compared to the non-cyclic precursors **12** or **15** (**14**). The extraannular triphenylene protons ortho to the acetylene (diacetylene) moiety are also shifted downfield, however, only by about 0.3 ppm. In the case of a paratropic ring current due to the formation of a formally (antiaromatic) 28 e-system we would expect an upfield shift for the latter protons. Therefore, we ascribe the observed NMR shift to a sterical compression of the protons inside **1** upon cyclization (as shown in the ESI†) (*c.f.*: B. F. Plummer, *Polycyclic Aromat. Compd.*, 1994, **4**, 25).
21 (*a*) G. C. McGonical, R. H. Bernhardt and D. J. Thomson, *Appl. Phys. Lett.*, 1990, **57**, 28; (*b*) J. P. Rabe and S. Buchholz, *Science*, 1991, **253**, 424; (*c*) K. Morishige, Y. Takami and Y. Yokota, *Phys. Rev. B: Condens. Matter*, 1993, **48**, 8277.
22 X. H. Qiu, C. Wang, Q. D. Zeng, B. Xu, S. X. Yin, H. N. Wang, S. D. Xu and C. L. Bai, *J. Am. Chem. Soc.*, 2000, **122**, 5550.
23 (*a*) W. Mamdouh, H. Uji-i, J. S. Ladislaw, A. E. Dulcey, V. Percec, F. C. De Schryver and S. De Feyter, *J. Am. Chem. Soc.*, 2006, **128**, 317; (*b*) S. De Feyter and F. C. De Schryver, *J. Phys. Chem. B*, 2005, **109**, 4290; (*c*) J. P. Rabe, S. Buchholz and L. Askadskaya, *Synth. Met.*, 1993, **54**, 339; (*d*) D. M. Cyr, B. Venkararaman and G. W. Flynn, *Chem. Mater.*, 1996, **8**, 1600; (*e*) L. Piot, D. Bonifazi and P. Samori, *Adv. Funct. Mater.*, 2007, **17**, 3689.
24 (*a*) C. A. Palma, M. Bonini, A. Llanes-Pallas, T. Breiner, M. Prato, D. Bonifazi and P. Samorí, *Chem. Commun.*, 2008, 5289; (*b*) S. Lei, K. Tahara, F. C. De Schryver, M. V. d. Auweraer, Y. Tobe and S. De Feyter, *Angew. Chem.*, 2008, **120**, 3006; (*c*) L. Kampschulte, T. L. Werblowsky, R. S. K. Kishore, M. Schmittel, W. M. Heckl and M. Lackinger, *J. Am. Chem. Soc.*, 2008, **130**, 8502; (*d*) K. Tahara, S. Okuhata, J. Adisoejoso, S. Lei, T. Fujita, S. De Feyter and Y. Tobe, *J. Am. Chem. Soc.*, 2009, **131**, 17583.
25 K. Becker, E. Da Como, J. Feldmann, F. Scheliga, E. T. Csanyi, S. Tretiak and J. M. Lupton, *J. Phys. Chem. B*, 2008, **112**, 4859.
26 E. Da Como, K. Becker, J. Feldmann and J. M. Lupton, *Nano Lett.*, 2007, **7**, 2993.
27 S. A. Jenekhe and J. A. Osaheni, *Science*, 1994, **265**, 765.
28 J. M. Lupton, I. D. W. Samuel, R. Beavington, P. L. Burn and H. Bässler, *Adv. Mater.*, 2001, **13**, 258.
29 M. J. Frisch, G. W. Trucks, H. B. Schlegel, G. E. Scuseria, M. A. Robb, J. R. Cheeseman, J. A. Montgomery, Jr, T. Vreven, K. N. Kudin, J. C. Burant, J. M. Millam, S. S. Iyengar, J. Tomasi, V. Barone, B. Mennucci, M. Cossi, G. Scalmani, N. Rega, G. A. Petersson, H. Nakatsuji, M. Hada, M. Ehara, K. Toyota, R. Fukuda, J. Hasegawa, M. Ishida, T. Nakajima, Y. Honda, O. Kitao, H. Nakai, M. Klene, X. Li, J. E. Knox, H. P. Hratchian, J. B. Cross, V. Bakken, C. Adamo, J. Jaramillo, R. Gomperts, R. E. Stratmann, O. Yazyev, A. J. Austin, R. Cammi, C. Pomelli, J. W. Ochterski, P. Y. Ayala, K. Morokuma, G. A. Voth, P. Salvador, J. J. Dannenberg, V. G. Zakrzewski, S. Dapprich, A. D. Daniels, M. C. Strain, O. Farkas, D. K. Malick, A. D. Rabuck, K. Raghavachari, J. B. Foresman, J. V. Ortiz, Q. Cui, A. G. Baboul, S. Clifford, J. Cioslowski, B. B. Stefanov, G. Liu, A. Liashenko, P. Piskorz, I. Komaromi, R. L. Martin, D. J. Fox, T. Keith, M. A. Al-Laham, C. Y. Peng, A. Nanayakkara, M. Challacombe, P. M. W. Gill, B. Johnson, W. Chen, M. W. Wong, C. Gonzalez and J. A. Pople, *Gaussian 03, Revision C.02*, Gaussian, Inc., Wallingford, CT, 2004.
30 B. D. Allen, A. C. Benniston, A. Harriman, I. Llarena and C. A. Sams, *J. Phys. Chem. A*, 2007, **111**, 2641.
31 Y. Yamaguchi, Y. Matsubara, T. Ochi, T. Wakamiya and Z. Yoshida, *J. Am. Chem. Soc.*, 2008, **130**, 13867.
32 (*a*) S. Klyatskaya, N. Dingenouts, C. Rosenauer, B. Müller and S. Höger, *J. Am. Chem. Soc.*, 2006, **128**, 3150; (*b*) K.-S. Moon, E. Lee and M. Lee, *Chem. Commun.*, 2008, 3061.
33 S. W. Provencer, *Comput. Phys. Commun.*, 1982, **27**, 229.
34 X. Feng, W. Pisula and K. Müllen, *J. Am. Chem. Soc.*, 2007, **129**, 14116.
35 S. Förster and C. Burger, *Macromolecules*, 1998, **31**, 879.
36 S. Förster, A. Timmann, M. Konrad, C. Schellbach, A. Meyer, S. S. Funari, P. Mulvaney and R. Knott, *J. Phys. Chem. B*, 2005, **109**, 1347.
37 (*a*) Y. J. Lin, Q. Cai, Q. F. Li, L. W. Xue, R. G. Yin and X. P. Yang, *J. Appl. Polym. Sci.*, 2010, **115**, 3393; (*b*) X. L. Feng, W. Pisula, T. Kudern, D. Q. Wu, L. J. Zhi, S. De Feyter and K. Müllen, *J. Am. Chem. Soc.*, 2009, **131**, 4439; (*c*) Y. L. Yang and C. Wang, *Curr. Opin. Colloid Interface Sci.*, 2009, **14**, 135.
38 In the bulk the cylinder–cylinder distance of 5.8 nm is smaller compared to the AFM-images, because on the substrate the alkyl-chains are nearly completely stretched due to adsorption to the interface.
39 N. Dingenouts, S. Klyatakaya, S. Rosenfeldt, M. Ballauff and S. Höger, *Macromolecules*, 2009, **42**, 5900.